An Efficient SAR Ground Moving Target Refocusing Method Based on PPFFT and Coherently Integrated CPF

DONG LI[1], (Senior Member, IEEE), CHENGXIANG ZHANG[1], HAINING MA[1], HONGQING LIU[2], (Senior Member, IEEE), JIA SU[3], (Member, IEEE), AND QINGHUA LIU[4]

[1]Center of Communication and Tracking Telemetering Command, Chongqing University, Chongqing 400044, China
[2]Chongqing Key Laboratory of Mobile Communications Technology, Chongqing University of Posts and Telecommunications, Chongqing 400065, China
[3]School of Electronics and Information, Northwestern Polytechnical University, Xi'an 710072, China
[4]Guangxi Key Laboratory of Wireless Wideband Communication and Signal Processing, Guilin University of Electronic Technology, Guilin 541004, China

Corresponding author: Dong Li (lid0705@cqu.edu.cn)

ABSTRACT The problem of ground moving target imaging and detection is difficult due to the large range cell migration (RCM) and time-varying Doppler frequency migration (DFM) in synthetic aperture radar (SAR) system. To finely refocus a moving target, motion parameters need be accurately estimated for compensating the RCM and DFM. In this work, an efficient ground moving target refocusing method based on pseudopolar fast Fourier transform (PPFFT) and coherently integrated cubic phase function (CICPF) is proposed without a priori knowledge of the motion parameters. First, based on the known radar platform motion parameters, the range curvature correction is completed, and then the range walk is corrected using the efficient PPFFT via estimating the slope of the range walk. In doing so, the energy of the moving target has been focused into the same range cell. Second, time-varying DFM parameters are obtained utilizing the proposed CICPF, and thus the well-focused result of the moving target is obtained. Compared with the existing methods, the proposed method has the advantages in computational complexity due to avoiding the searching and interpolation operation, and anti-noise performances thanks to fully exploiting the two-dimensional (2-D) coherently accumulation characteristics and the energy of all the scatterers in moving target for estimating motion parameters. Finally, both the simulated and real SAR data processing results are presented to validate the proposed method.

INDEX TERMS Synthetic aperture radar (SAR), ground moving target refocusing, pseudopolar fast Fourier transform (PPFFT), coherent integrated cubic phase function (CICPF).

I. INTRODUCTION

Synthetic aperture radar (SAR) has been widely adopted in many fields of civil and military applications because it has the capacity to obtain high-resolution images regardless the weather condition, day and night [1]–[3]. It is also well-known that longer synthetic aperture time produces high resolution images of ground moving targets, which is beneficial

The associate editor coordinating the review of this article and approving it for publication was Nagendra Prasad Pathak.

to subsequent classification and recognition [4]. However, the complex motion of the moving target over a long period of time causes large range cell migration (RCM) and Doppler frequency migration (DFM), which results in defocused and dislocated targets [5], [6]. Therefore, it is important to accurately compensate RCM and DFM for obtaining the well-focused moving target SAR image.

In this work, the main components of RCM consist of range walk (i.e., linear RCM) and range curvature (i.e., quadratic RCM), and higher order components are assumed

to be insignificant. In recent years, many approaches have been proposed to obtain the image of ground moving target with SAR system, and they can be mainly classified into four groups. The first kind is the Keystone transform (KT) based methods [7]–[13], such as first-order Keystone transform [7]–[9], second-order Keystone transform (SOKT) [10], [11], Doppler Keystone [12], Deramp-Keystone [13], etc. These methods adjusted the slow time axis to eliminate the coupling between the distance and the slow time, and to conduct the RCM correction when the target's motion parameters are unknown. However, they require interpolation operation, which is of high computational complexity and known to be inaccurate. The second group is the Radon transform (RT) based methods [14]–[18], such as Radon transform [14], Radon-Fourier transform (RFT) [15], Radon-fractional Fourier transform [16], Radon ambiguity function [17] and Radon Wigner-Ville distribution (WVD) [18], etc. Although the RT based algorithms are effective, they need to constantly adjust the search angle and range step to obtain precision estimations, which means a trade-off must be made between accuracy and computational complexity. The third class is the joint time-frequency analysis based methods including short time Fourier transform [19], WVD [20], ambiguity function (AF) [21], and fractional Fourier transform (FrFT) [22], [23], etc. These methods handle a time-varying signal with the low time-frequency resolution and usually require high signal noise ratio (SNR) condition. Since the nonlinear transform is used, the cross-terms interference can also be problematic. In the last group, the prior information of the certain properties in the SAR system are exploited, and representatives are stationary-phase-based two-dimensional (2-D) matched filtering method [24], geometry-information-aided method [25], and symmetric Doppler views based approach [26]. However, prior information is not easy to obtain in real applications, which limits the practicality of such methods. More recently, a novel method, termed as gradient feature method (GFM) [27], is proposed to estimate the slope of the range walk via exploiting the RCM geometry information. Although this method obtains the motion parameters with a low computational complexity, it is sensitive to noise. From the aforementioned analysis, the existing RCM correction algorithms still suffer from either high computational complexity or the requirement of high SNR condition. Therefore, a further study for efficient RCM correction method under the low SNR environment is still necessary.

After the range compression and the RCM correction, the energy of moving target is concentrated into the same range cell and it appears as a linear frequency modulated form. Based on that, the parameter estimation methods can be developed to estimate the time-varying Doppler parameters, for example, second-order Wigner-Ville Distribution (SoWVD) [9] and fractional Fourier transform (FrFT) [28], [29], high-order ambiguity function (HAF) [30], discrete polynomial-phase transform (DPT) method [31], Lv's Distribution method (LVD) [32], to name

a few. However, in practice, the performance of WVD-based methods is limited by cross-terms interference and spurious peaks caused by its nonlinear feature, and cannot be regarded as the real characteristic of the linear frequency modulation (LFM) signal. The FrFT method avoids the influence of cross-terms and spurious peaks, but it has a high computational complexity due to the search operation used along the frequency modulate rate. The HAF method via one-dimensional search based on multiple non-linear operations to obtain phase parameters saves a great amount of computations, but it requires high input SNR. The DPT method adopts a preliminary compensation of the modulation frequency to obtain the modulation parameters, which indicates a low computational load. However, its accuracy of parameter estimation severely depends on the construction of the compensation function. The LVD method better suppresses cross-terms and spurious peaks for multiple LFM signal parameter estimation. It suffers from a high computational complexity and accuracy loss caused by the interpolation operation. There are some other approaches, for example, sparse signal reconstruction concept based motion parameter estimations specifically for multi-target scenario [33], [34], have been studied as well. It is well-known that these methods are time-consuming and sensitive to noise. Recently, the instantaneous frequency estimation method based on cubic phase function (CPF) is proposed in [35]–[38]. For the single component case, the CPF method is demonstrated to be effective [35], [36]. However, there are spurious peaks and cross-terms dealing with multicomponent LFM signal, which seriously affects the parameter estimation performance. To suppress the cross terms and spurious peaks, in [37], [38], the product CPF (PCPF) and the integral CPF (ICPF) are proposed, but they only use the partial auto-term energy and amplitude information, which limits the noise suppression performance. To conclude, the current approaches still suffer from heavy computational burden and/or performance loss in low SNR scenario.

To overcome these issues, in this work, we propose an efficient moving target refocusing method based on pseudopolar fast Fourier transform (PPFFT) and coherent integrated CPF (CICPF). The method first uses the radar platform motion parameters to conduct the range curvature correction. After that, the efficient PPFFT is developed to estimate the slope of the range walk trajectory under a low SNR environment, and with the obtained radial velocity, the energy of moving target is concentrated into one range cell. After the RCM correction, the time-varying Doppler parameter is modeled as a multiple LFM signal, and the CICPF is then applied to obtain the motion parameters of the moving target. Using the estimated motion parameter, the high-order term DFM compensation is performed and the well-focused result of the moving target is thus obtained. The computational cost analysis is provided to show the efficiency of the proposed method. The simulations and experiments on the real data demonstrate the great performance improvements over the state-of-the-art algorithms, especially under the low SNR case.
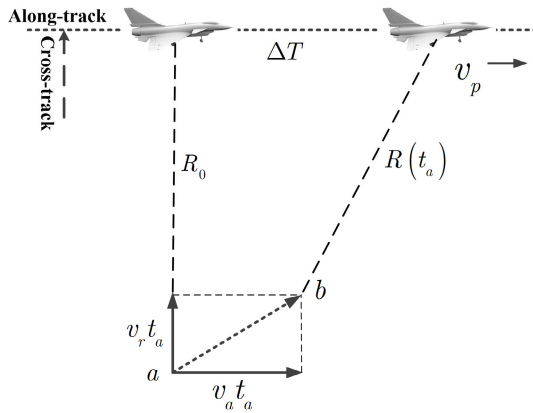
FIGURE 1. The geometric model of airborne SAR imaging system.

This remainder of paper is organized as follows. In section II, the airborne SAR moving target imaging geometry and signal model are presented. The principles of the proposed method are described in details in section III. Section IV shows the simulation and real data process results to demonstrate the validity of the proposed methods. Section V concludes this paper.

II. AIRBORNE SAR MOVING TARGET IMAGING GEOMETRY AND SIGNAL MODEL

In the 2-D slant plane, with a side-looking work mode, the geometry between a flying platform with velocity v_p and the moving target is depicted in Fig 1. During the slow time interval ΔT, the moving target travels from point a to point b in which v_a and v_r respectively represent the along-track velocity and cross-track velocity of the moving target. The R_0 and $R(t_a)$ denote the nearest slant ranges and instantaneous slant range between the platform and target, and t_a is the azimuth slow time variable.

Employing the LFM signal as the transmitted signal and after range compression, the received signal of a moving target is [4]–[9]

$$s(t_r; t_a) = \sigma G \sin c \left[B_r \left(t_r - \frac{2R(t_a)}{c} \right) \right] w_a(t_a)$$
$$\times \exp \left[-j \frac{4\pi}{\lambda} R(t_a) \right] \quad (1)$$

where t_r is the range fast-time variable, σ is the complex reflectivity of the target, G is the range compression gain, $w_a(\cdot)$ is the azimuth window function, λ is the wavelength of the transmitted signal, c is the speed of light, and B_r is the bandwidth of the transmitted signal. Based on the geometry relationship in Fig.1, the instantaneous range $R(t_a)$ is expanded into the second-order term model via the Taylor series expansion, given by

$$R(t_a) = \sqrt{(v_p t_a - v_a t_a)^2 + (R_0 - v_r t_a)^2}$$
$$\approx R_0 + b_1 t_a + b_2 t_a^2 \quad (2)$$

where b_1 and b_2 respectively represent the equivalent first- and second-order coefficients of the instantaneous slant $R(t_a)$. In this work, the higher-order terms of phase are ignored because of the relationship $(v_p - v_a) t_a \ll R_0$. In (2), the expressions of b_1 and b_2 are

$$b_1 = -v_r, \quad b_2 = \frac{(v_p - v_a)^2}{2R_0} \quad (3)$$

Substituting (2) and (3) into (1), and performing fast Fourier transform (FFT) with respect to t_r yields

$$s(f_r; t_a) = \sigma_s G w_a(t_a) W(f_r) \exp \left[-j \frac{4\pi R_0}{\lambda} \right] \exp \left(j \frac{4\pi v_r}{\lambda} t_a \right)$$
$$\exp \left\{ -j \frac{4\pi}{\lambda} \left[\frac{(v_p - v_a)^2}{2R_0} \right] t_a^2 \right\} \exp \left\{ -j \frac{4\pi R_0}{c} f_r \right\}$$
$$\exp \left\{ j \frac{4\pi v_r}{c} f_r t_a \right\} \exp \left\{ -j \frac{4\pi}{c} \left[\frac{(v_p - v_a)^2}{2R_0} \right] f_r t_a^2 \right\}$$
$$(4)$$

where f_r is the range frequency variable corresponding to the t_r, and $W(\cdot)$ is the envelope of the range frequency. From (4), it is seen that the first and the fourth terms have no effect on the subsequent analysis and will be ignored. The second exponential term indicates the Doppler centroid shift. The third exponential term tells that the Doppler modulate rate of the fast moving target is mainly affected by the along-track velocity. The fifth and sixth exponential terms are called range walk and range curvature term, respectively, and they are the reasons that the trajectory of the moving target spreads over several range cells. Therefore, if one wants to produce a well-focused image of a moving target as well as its motion parameters, the RCM should be corrected first.

III. PROPOSED METHOD
In this section, the procedures of the proposed PPFFT and CICPF algorithm for airborne SAR ground moving target imaging and parameters estimation are described. However, prior to the time-varying DFM compensation, the RCM correction is performed as follows.

A. RCM CORRECTION BASED ON PPFFT
In practice, since the motion of the moving targets is non-cooperative, the target signal is usually buried in strong and complex airborne clutter, and high resolution imaging requires a long coherent integration time leading to large range curvature. In this scenario, after range compression, the envelope of different targets overlaps with each other and it is not easy to isolate each target and determine their motion parameters, demonstrated in Fig 2. In this work, the match-filter method is utilized to correct the range curvature of the moving target, which is based on the fact that the along-track velocity of the moving target v_a is much smaller than the velocity of platform v_p. The match-filter function for range
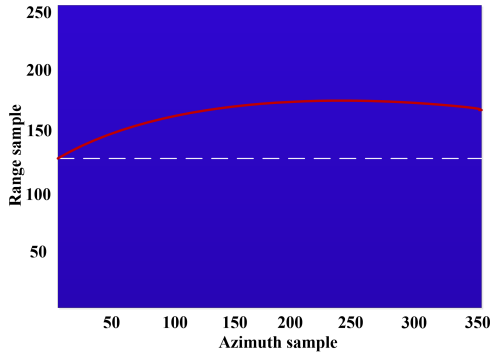
FIGURE 2. RCM with range curvature and range walk.
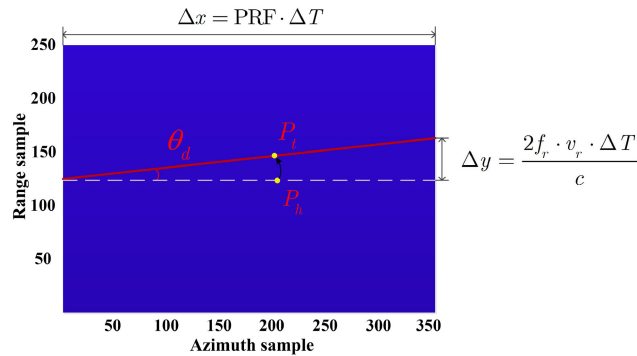
FIGURE 3. The range walk illustration.

curvature correction is given by

$$H_{\text{RCM}} = \exp\left\{j\frac{4\pi}{c}\left[\frac{(v_p - v_a)^2}{2R_0}\right]f_r t_a^2\right\}$$

$$\approx \exp\left(j\frac{2\pi v_p^2}{cR_0}f_r t_a^2\right) \quad (5)$$

After the range curvature correction, the effects of platform velocity and target along-track velocity on the range curvature can be well eliminated, and the trajectory of the moving target is focused into a slope line, demonstrated in Fig 3. It is also noted that the compensation of the range walk simply means to estimate the trajectory slope in the $t_r - t_m$ plane. There are several approaches that conducts this estimation, for example, KT [7]–[9], RT [14], [25], Hough transform [21]. However, they are known to be of high computational complexity and performance loss due to the interpolation and search operation. To overcome those issues, in this work, the geometric information of the linear trajectory in the $t_r - t_m$ plane is exploited to efficiently estimate the trajectory slope associated with range walk according to the peak coordinate. With the estimated b_1, the range walk can be accurately compensated.

During ΔT, the cross and along-track motion distances of the moving target are respectively expressed as

$$\Delta x = \text{PRF} \cdot \Delta T \quad (6)$$
$$\Delta y = 2f_r v_r \Delta T / c \quad (7)$$
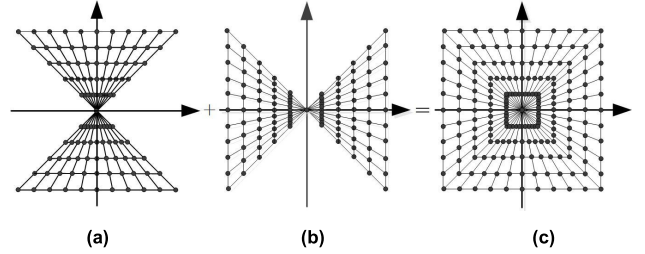
FIGURE 4. The pseudopolar sampling grids. (a) The pseudopolar sectors P_1. (b) The pseudopolar sectors P_2. (c) The pseudopolar grids $P = P_1 \cup P_2$.

where PRF is pulse repetition frequency. Therefore, the slope of the range walk is calculated by

$$\tan \theta_d = \frac{\Delta y}{\Delta x} = \frac{2f_r \cdot v_r}{\text{PRF} \cdot c} \quad (8)$$

where θ_d represents the trajectory slope between the trajectory and the horizontal line. If the value of θ_d is estimated as $\hat{\theta}_d$, the cross-track velocity is obtained as

$$\hat{v}_r = \frac{\text{PRF} \cdot \tan \hat{\theta}_d \cdot c}{2f_r} \quad (9)$$

From (9), it is seen that the key step now is to efficiently estimate the trajectory slope.

Assume a point $P_t (X_t, Y_t)$ in range walk trajectory, the corresponding point is $P_h (X_h \ Y_h)$ in the horizontal line, shown in Fig 3. The relationship of $P_t (X_t, Y_t)$ and $P_h (X_h \ Y_h)$ is

$$[X_t \ Y_t]^T = \begin{bmatrix} \cos \theta_d & -\sin \theta_d \\ \sin \theta_d & \cos \theta_d \end{bmatrix} [X_h \ Y_h]^T \quad (10)$$

where θ_d is the rotating angle. According to (10), this relationship demonstrates that the range walk trajectory is a rotated version of the horizontal line. Moreover, the corresponding polar Fourier transform (PFT) relationship in the polar coordinate is [39]

$$I_t^{\text{PFT}}(r, \theta) = I_h^{\text{PFT}}(r, \theta + \theta_d) \quad (11)$$

where $I_t^{\text{PFT}}(r, \theta)$ and $I_h^{\text{PFT}}(r, \theta)$ are PFTs of the range walk trajectory and the horizontal line, respectively. Observing (11) reveals that the rotation of two line trajectories in the image domain corresponds to the translation along the polar angle. Therefore, using this relationship, the rotating angle θ_d can be estimated in the polar coordinate domain. In [39], a 2D Fourier transform (FT) and polar coordinate mapping methods are proposed to transform the rotation into the translation at polar coordinate via an interpolation operation to estimate rotating angle θ_d. However, the resampling of Cartesian frequency values on a polar grid is sensitive to the interpolation and the estimation accuracy of θ_d is thus degraded by the approximation errors. Additionally, the computational load is also high due to the interpolation operation [39]. To reduce the computations and increase the estimation accuracy, we propose an efficient method that requires no interpolations to perform range walk correction by a use of PPFFT.

To address the absence of fast implementation for the PFT, a different sampling grid is developed. In the sampling grids,

the rotation motion estimation should become a translational estimation, and 2D FT under the designed sample grid can be efficiently implemented without the interpolation operation. To that aim, in this work, the pseudopolar Fourier transform (PPFT) is utilized, whose grid approximates the polar grid, shown in Fig 4(c). The pseudopolar grid P is defined by the set of samples [40], [41]

$$P \triangleq P_1 \cup P_2 \quad (12)$$

where

$$P_1 \triangleq \left\{ \left(-\frac{2l}{N}k, k \right) \mid -\frac{N}{2} \le l \le \frac{N}{2}, -N \le k \le N \right\} \quad (13a)$$

$$P_2 \triangleq \left\{ \left(k, -\frac{2l}{N}k \right) \mid -\frac{N}{2} \le l \le \frac{N}{2}, -N \le k \le N \right\} \quad (13b)$$

To visually observe sets P_1 and P_2, pseudopolar grids are provided in Fig 4. In Fig 4a and 4b, k and l, respectively, act as a "pseudo-radius" and a "pseudo-angle". The resolution of the pseudopolar grid is $N + 1$ in the angle direction and $2N + 1$ in the radial direction. Using (r, θ) representation, the pseudopolar grid is

$$P_1 (k, l) = \left(r_k^1, \theta_l^1 \right), P_2 (k, l) = \left(r_k^2, \theta_l^2 \right) \quad (14)$$

where $k = -N, \ldots, N$, $l = -N/2, \ldots, N/2$, $r_k^1 = k\sqrt{4\left(l/N\right)^2 + 1}$, $r_k^2 = k\sqrt{4\left(l/N\right)^2 + 1}$, $\theta_l^1 = \pi/2 - \arctan\left(2l/N\right)$, $\theta_l^2 = \arctan\left(2l/N\right)$. Let PPFT be the samples of the FT on the pseudopolar grid P, and the PPFT $\hat{I}_{PP}^j (j = 1, 2)$ is a linear transformation, which is defined by [41].

$$\hat{I}_{PP}^1 (k, l) \triangleq I \left(-\frac{2l}{N}k, k \right) = \sum_{u,v=-N/2}^{N/2-1} I (u, v) e^{-\frac{2\pi i}{M} \left(-\frac{2l}{N} ku + kv \right)}$$

$$\hat{I}_{PP}^2 (k, l) \triangleq I \left(k, -\frac{2l}{N}k \right) = \sum_{u,v=-N/2}^{N/2-1} I (u, v) e^{-\frac{2\pi i}{M} \left(ku - \frac{2l}{N} kv \right)}$$

$$(15)$$

From Fig 4c, for each fixed angle, the samples of the pseudopolar grid are uniformly spaced in the radial direction. However, for different angles, the spacing varies. Moreover, the grid is not equally spaced in the angular direction, but has equally spaced angles. That is

$$\Delta \tan \theta_{pp}^1 (l) \triangleq \cot \theta_{l+1}^1 - \cot \theta_l^1 = \frac{2}{N}$$

$$\Delta \tan \theta_{pp}^2 (l) \triangleq \tan \theta_{l+1}^2 - \tan \theta_l^1 = \frac{2}{N} \quad (16)$$

The important properties of the PPFT are that it is invertible and both the forward and inverse PPFT are implemented using fast algorithms [42]. In [42], the fast implementation only needs one-dimensional FFT and the FrFT, which means the PPFFT has a low computational complexity.

The PPFFT is conducted on the image after range curvature correction and its result is denoted by $M (r_k, \theta_l)$. According to (10) and (11), the relationship between $M (r_k, \theta_l)$ and the horizontal line in the pseudopolar sampling grid has been transformed to the translational motion along the pseudo-angle in the pseudopolar coordinate system. The horizontal line corresponds to the middle position of the pseudo-angle dimension. Therefore, the rotation angle $\hat{\theta}_d$ is estimated by (17), as shown at the bottom of this page where N_p is the number of pseudo-angle dimension sampling point, $m = 1, 2, \ldots, N$, $\sum_{k=1}^{N} M (r_k, \theta_l)$ is the radial integration of the image after PPFFT operation. Substituting $\hat{\theta}_d$ into (9), the radial velocity $\hat{v}_r$ is readily obtained, and the range walk correction filter in the range-frequency domain is

$$H_{\text{RWM}} = \exp \left(-j\frac{4\pi \hat{v}_r}{c} f_r t_a \right) \quad (18)$$

After RCM correction, the same scatterer energy of moving target is concentrated into one certain range cell and the time-varying Doppler signal is characterized as an LFM signal. To produce a high-resolution, the parameters of the LFM signal need to be accurately estimated as well. In real applications, the received echo data are usually of low SNR due to the long distance or the stealth characteristic of the moving target. Therefore, low SNR environment needs to be taken into account when developing LFM parameter estimations.

B. ALONG-TRACK MOTION PARAMETER ESTIMATION BASED ON CICPF

According to the above analysis, after RCM correction, the resulting signal can be represented by LFM, and without losing generality, the K component LFM signal containing noise is used as

$$s (t_a) = \sum_{k=1}^{K} \sigma_k \exp \left[-j\frac{4\pi}{\lambda} \left(b_{k,0} + b_{k,1} t_a + b_{k,2} t_a^2 \right) \right] + n (t_a) \quad (19)$$

where $n (t_a)$ consists of the complex zero-mean white Gaussian noise with variance δ^2 and the clutter.

To obtain the chirp rate $b_{k,2}$, many parameter estimation methods are developed such as SoWVD method [9], FrFT method [28], [29], HAF method [30], DPT method [31], LVD

$$\hat{\theta}_d = \begin{cases} \arctan \left[\left(\arg \max_m \left(\sum_{k=1}^{N} M (r_k, \theta_l) \right) - \frac{N_p}{2} \right) \times 4 \Big/ N_p \right], & \hat{\theta}_d \in \left[0, \frac{\pi}{2} \right) \\ \pi + \arctan \left[\left(\arg \max_m \left(\sum_{k=1}^{N} M (r_k, \theta_l) \right) - \frac{N_p}{2} \right) \times 4 \Big/ N_p \right], & \hat{\theta}_d \in \left[\frac{\pi}{2}, \pi \right) \end{cases} \quad (17)$$
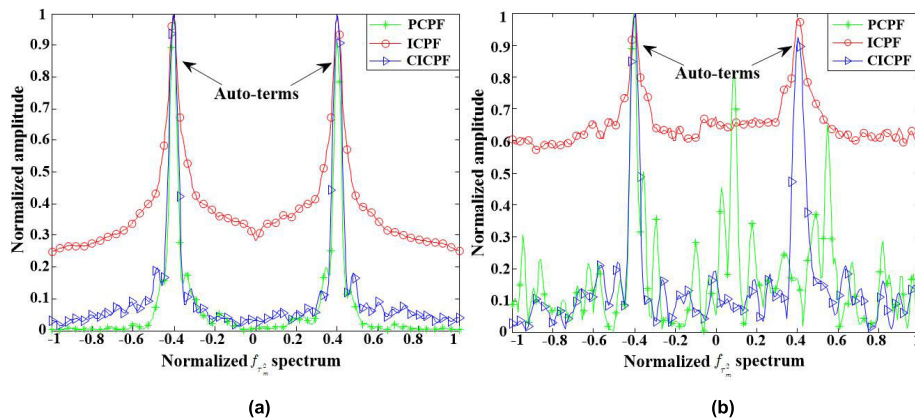
FIGURE 5. Comparisons of CICPF, PCPF and ICPF. (a) SNR=5dB. (b) SNR= −5dB.

TABLE 1. Parameters of each component.

Parameters Name	σ_k	$b_{k,0}$	$b_{k,1}$	$b_{k,2}$
$k=1$	1.0	0	0.1π	$0.4\pi/N$
$k=2$	1.0	0	-0.1π	$-0.4\pi/N$

method [32], CPF method [36], the PCPF method [37] and the ICPF method [38]. However, they are either of the heavy computational burden and/or suffer from performance loss in low SNR scenario. It is shown that in [43], our proposed the CICPF approach is effective under the low SNR case, and the CICPF of (19) is

$$
\begin{aligned}
\text{CICPF}\left(f_{t_a}; f_{\tau_a^2}\right) &= \Gamma_{t_a}\left[s\left(t_a\right), \tau_a\right] \\
&= \iint s\left(t_a + \tau_a\right) s\left(t_a - \tau_a\right) \exp\left[-j2\pi f_{t_a} t_a\right] \\
&\quad \times \exp\left[-j2\pi f_{\tau_a^2}\left(t_a^2 + \tau_a^2\right)\right] dt_a d\tau_a^2 \\
&= \sigma\,\delta_{t_a}\left(f_{t_a} - 2b_{k,1}\right)\delta_{\tau_a^2}\left(f_{\tau_a^2} - 2b_{k,2}\right) \quad (20)
\end{aligned}
$$

where Γ_{t_a} is used to denote the CICPF operator, τ_a denotes the lag-time variable, f_{t_a} is the frequency variable with respect to t_a, $f_{\tau_a^2}$ is the frequency variable with respect to τ_a^2, σ denotes the signal amplitude in the CICPF domain, and $\delta\left(\cdot\right)$ denotes the Dirac delta function. From (20), one observes that after CICPF, there is a well-focused peak at $\left(2b_{k,1},\ 2b_{k,2}\right)$ in the CICPF domain $\left(f_{t_a}; f_{\tau_a^2}\right)$.

To demonstrate the noise tolerance performance of the CICPF, a two-component LFM signal with parameters listed in Table 1 is adopted, and then it is corrupted by complex additive white Gaussian noise with different SNRs of 5dB and −5dB. The comparisons of the CICPF, PCPF [37] and ICPF [38] are provided in Fig 5(a) and Fig 5(b), respectively. In the high SNR case, the CICPF, PCPF and ICPF (the different time indices are $L = 5$ and selected time positions of $[-100\ {-50}\ 0\ 50\ 100]$), they all demonstrate the

capacity of suppressing the cross-terms and spurious peaks, shown in Fig 5(a). However, in the case of low SNR, spurious peaks are present in the PCPF, shown in Fig 5(b). Both ICPF and CICPF can suppress the spurious peaks and form two distinct peaks for auto-terms, but the sidelobes of the CICPF indicate that its noise suppression ability should be better than that of the ICPF. In addition to that, it should be noticed that CICPF is realized by NUFFT [43], and thus it is more computationally efficient.

By a use of estimated $b_{k,1}$ and $b_{k,2}$, the compensation function is designed by

$$
H_{Azimuth} = \exp\left(j\frac{4\pi}{\lambda}\left(b_{k,1}t_a\right) + j\frac{4\pi}{\lambda}\left(b_{k,2}t_a^2\right)\right) \quad (21)
$$

By multiplying equation (19) and (21), the azimuth DFM compensation is completed. Finally, performing azimuth FFT, the moving target refocusing is produced. The detailed implementation flow chart of the proposed method is given in Fig 6.

C. COMPUTATIONAL COMPLEXITY ANALYSIS
In this section, the computational complexity of the proposed method is analyzed and compared with SoWVD method [9], Radon transform method (RTM) [29] and GFM [27]. Suppose that the range sampling point is N_r and the azimuth sampling point is N_a, and for a signal of length N, the computational complexity of FFT is $O\left(N\log_2 N\right)$.

The SoWVD method conducts RCM correction based on KT and along-track moving parameter estimation. Based on its descriptions, the computational cost consists of the following steps. First, using the match-filter to achieve the range curvature correction, and its computational complexity is $O\left(N_r N_a\right)$. Second, performing KT to accomplish range walk correction including coordinate transformation and interpolation operations, the computational complexity is $O\left(2\left(2N_{ker} - 1\right)N_r N_a\right)$, where N_{ker} is the length of the interpolation kernel. And then, performing SoWVD to estimate the along-track moving parameter, the computational
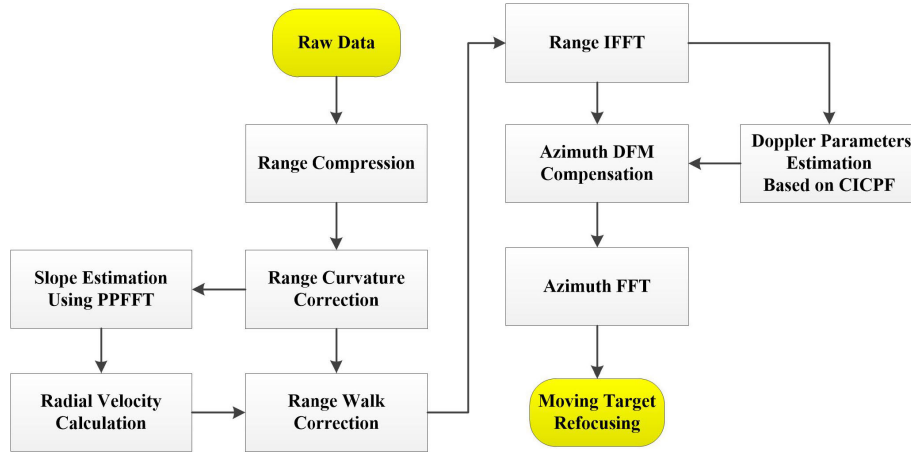
FIGURE 6. Flowchart of the proposed method.

complexity is $O\left(2N_aN_a\log_2 N_a\right)$. Therefore, the total computation burden of SoWVD method is

$$C_{\text{SoWVD}} = O\left(N_rN_a + 2\left(2N_{\text{ker}} - 1\right)N_rN_a \right.$$
$$\left. +2N_aN_a\log_2 N_a\right) \qquad (22)$$

For RTM approach, first, it also uses the match-filter to achieve the range curvature correction, and its computational complexity is $O\left(N_rN_a\right)$. Second, performing RT to obtain the slope of range walk to achieve the range walk correction, this processing includes $\rho - \theta$ coordinate transformation and search maximum to obtain the principal direction. The computational complexity of coordinate transformation is $O\left(N_\theta N_rN_a\right)$, and the computational complexity of the principal direction estimation is $O\left(N_rN_\theta\right)$, where N_θ is the number of the angle direction sampling points. After that, performing FrFT to obtain the target moving coefficients, since the N_a-dimensional fast discrete FrFT requires $O\left(N_a\log_2 N_a\right)$ computation, the FrFT complexity will be $O\left(N_{\text{FrFT}}N_a\log N_a\right)$, where N_{FrFT} is the total number of FrFT in the scanning. Therefore, the total the computation burden of RTM is

$$C_{\text{RTM}} = O\left(2N_rN_a + N_\theta N_rN_a + N_rN_\theta \right.$$
$$\left. +N_{\text{FrFT}}N_a\log_2 N_a\right) \qquad (23)$$

The GFM also includes the RCM correction and along-track moving parameter estimation based on the LVD. Frist, the computational complexity of match-filter is the same as $O\left(N_rN_a\right)$. Second, the computational complexity of the construction of a covariance matrix and eigen-decomposition of the covariance matrix is $K^2N_rN_a$, and the computational complexity of the feature vector is K^3, where K is the dimension of the feature vector. After that, LVD is performed to obtain the moving coefficients, and its computational cost consists of the scaled FT and the 2-D FFT of the parametric symmetric instantaneous autocorrelation function and the computation burden is about $O\left(2N_aN_a\log_2 N_a\right)$. Therefore,

the total computation cost of GFM is

$$C_{\text{GFM}} = O\left(2N_rN_a + K^2N_rN_a + K^3 \right.$$
$$\left. +2N_aN_a\log_2 N_a\right) \qquad (24)$$

According to the flowchart of the proposed method in Fig 6, the computational load of the proposed method mainly involves following steps. First, the match-filter operation is $O\left(N_rN_a\right)$. Second, performing PPFFT to obtain the slope of range walk to achieve the range walk correction, the computational complexity of PPFFT is $O\left(N_rN_a\log_2 N_r\right)$, and the computational complexity of the slope estimation is N_a. Third, performing CICPF to obtain the target moving coefficients, its computation burden is $O\left(2N_aN_a\log_2 N_a\right)$. To summarize, the total computation cost of the proposed method is

$$C_{\text{proposed}} = O\left(2N_rN_a + N_rN_a\log_2 N_r + N_a \right.$$
$$\left. +2N_aN_a\log_2 N_a\right) \qquad (25)$$

From (22), (23), (24) and (25), one observes that the computational complexity of the proposed method is slightly larger than the GFM, but it is smaller than that of SoWVD method and RTM. Moreover, the computational advantage is more obvious as N_{ker}, N_θ and N_{FrFT} increase in previous methods.

IV. EXPERIMENTAL RESULTS AND ANALYSIS
A. SLIMULATION RESULTS AND ANALYSIS
In this section, simulated data are generated to demonstrate the effectiveness of the proposed method. The target motion parameters are $v_r = -8m/s$, $v_a = 3m/s$, the radar transmits a LFM signal, and the parameters for the SAR system is given in Table 2.

Fig 7(a) shows the result of range compression, it is seen that the moving target has a significant RCM. Fig 7(b) shows the result of the range curvature correction, after the range curvature correction, the echo envelope appears as a slanted
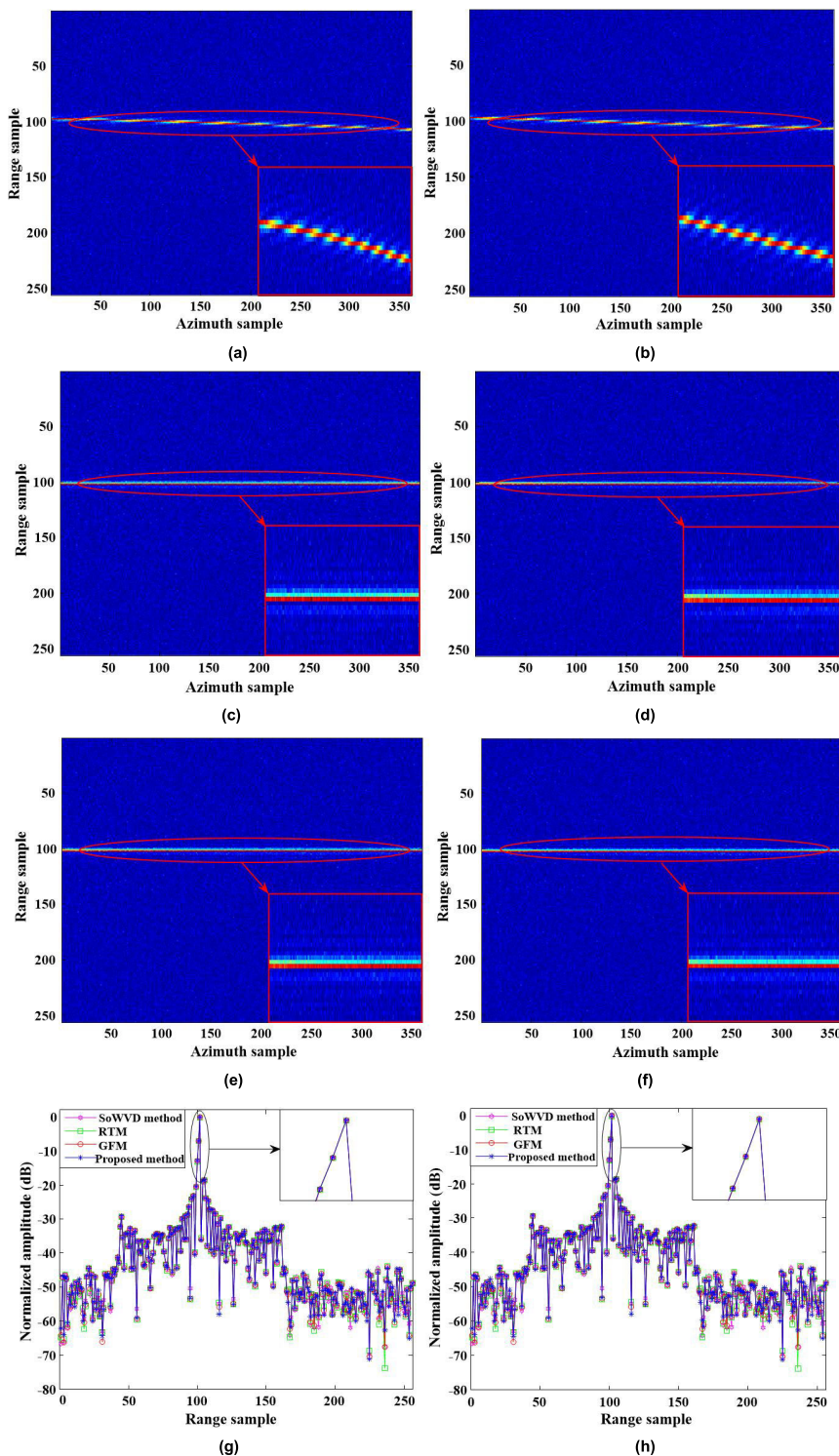
FIGURE 7. Simulation results. (a) The result of range compression. (b) The result of range curvature correction. (c) The result of range walk correction using the KT method. (d) The result of range walk correction using the RT method. (e) The result of range walk correction using the GFM. (f) The result of range walk correction using the PPFFT method. (g) Range focusing results of moving target by the SoWVD method, RTM, GFM, and the proposed method. (h) Azimuth focusing results of moving target by the SoWVD method, RTM, GFM, and the proposed method.

straight line. Based on this, the angle of the line is estimated using PPFFT, and the result of range walk correction is given in Fig 7(f). To compare, range walk correction results

obtained by KT, RT, and GFM are respectively depicted in Fig 7(c), Fig 7(d), and Fig 7(e). It is observed that the proposed method has the best correction effect.
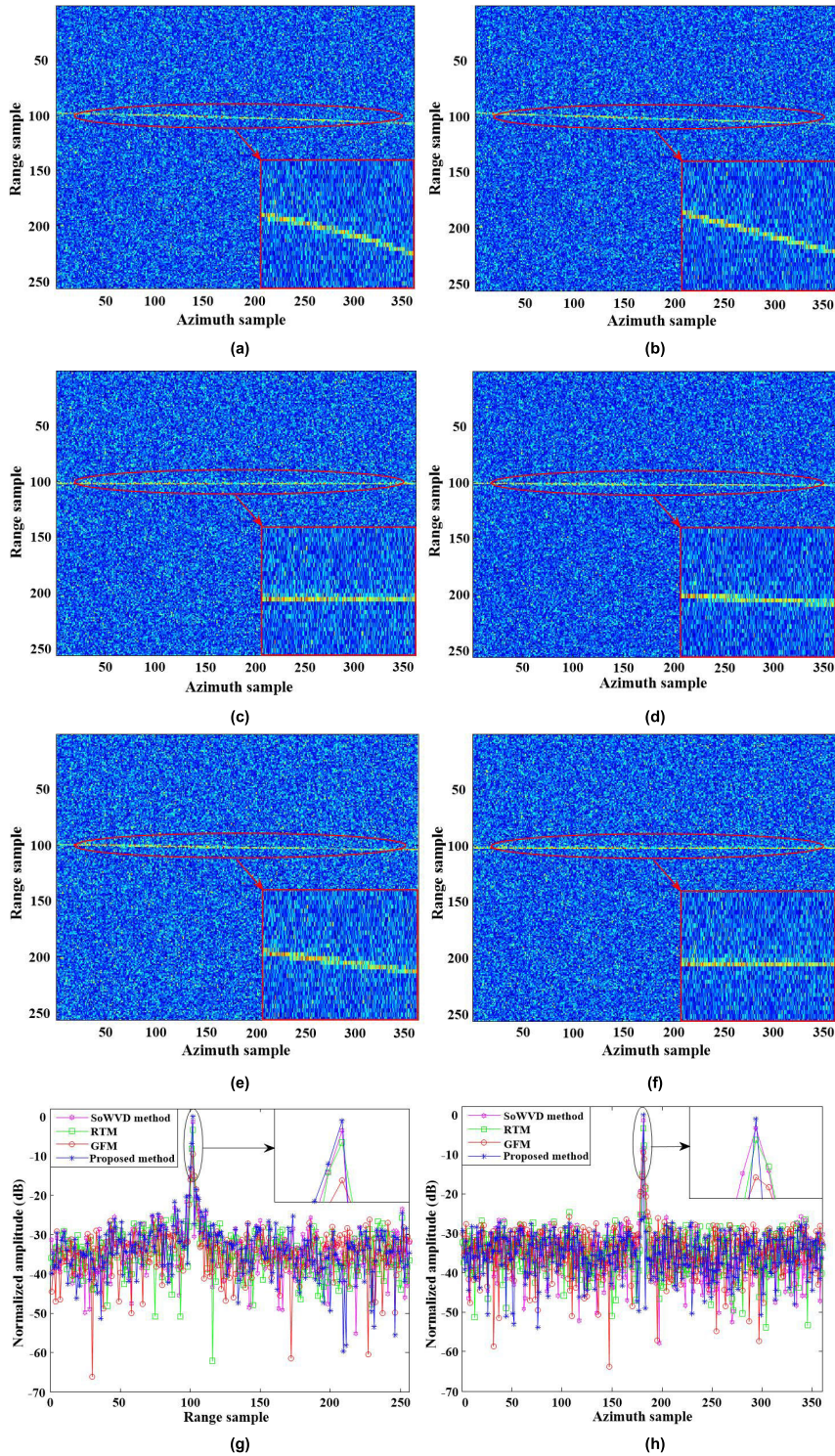
FIGURE 8. Simulation results. (a) The result of range compression. (b) The result of range curvature correction. (c) The result of range walk correction using the KT method. (d) The result of range walk correction using the RT method. (e) The result of range walk correction using the GFM. (f) The result of range walk correction using the PPFFT method. (g) Range focusing results of moving target by the SoWVD method, RTM, GFM, and the proposed methods. (h) Azimuth focusing results of moving target by the SoWVD method, RTM, GFM, and the proposed method.

After the RCM correction is completed, the CICPF is employed to estimate the values of the first-order and second-order motion parameters, and utilizing the estimated

parameters to accomplish azimuth DFM compensation, the imaging result is obtained. In Fig 7(g), the comparisons of range focusing results of moving target obtained by SoWVD
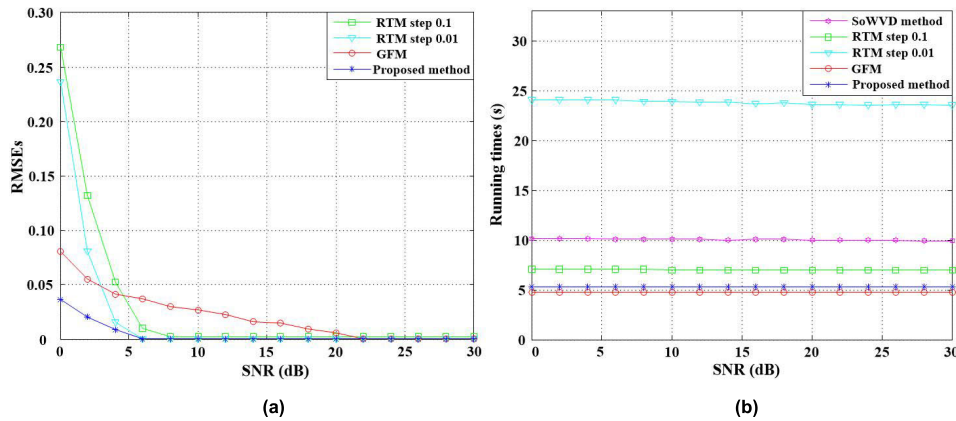
FIGURE 9. Performance comparison. (a) RMSEs of the estimated angle versus SNR. (b) The running times versus SNR.

TABLE 2. SAR system parameters.

Parameters name	Value
Carrier frequency	5GHz
Range sample frequency	600MHz
Pulse duration time	0.1us
Nearest slant range	1000m
Range bandwidth	500MHz
Pulse repetition frequency	1000Hz
SAR platform velocity	150m/s
Dwell time	0.3s

TABLE 3. X-band radar system parameters.

Parameters name	Value
Carrier frequency	8.85GHz
Range sample frequency	60MHz
Pulse duration time	10us
Aperture size	0.56m
Range bandwidth	40MHz
Pulse repetition frequency	1000Hz
SAR platform velocity	120m/s
Swath central range	9000m

method, RTM, GFM, and the proposed method are provided, while the azimuth focusing results obtained by the SoWVD method, RTM, GFM, and the proposed method are depicted in Fig 7(h). It can be seen that the focus of the proposed method is the same as the existing methods in the case of high SNR (25dB in this case), which validates the effectiveness of the proposed method.

To verify the performance of the proposed method in low SNR case, the simulation experiment is conducted with 5 dB SNR. The range walk corrections obtained by different approaches are demonstrated in Fig 8(c)-(f). From the results, the proposed approach outperforms others by clearly transforming the energy into one range cell. In Fig 8(g)-(h), the range and azimuth focusing results obtained by SoWVD method, RTM, GFM, and the proposed method are depicted. The proposed method produces the same quality focusing as SoWVD method, but with a lower computational complexity.

To objectively measure the performances of different approaches, the root mean square errors (RMSEs) of the estimated angle by the RTM, GFM and the proposed method versus SNR are provided in Fig 9(a), where the RMSE values are obtained by averaging 100 independent noise realizations. The proposed method has the lowest SNR threshold, which agrees with the previous studies. The running times of different approaches versus SNR are presented in Fig 9(b), where Intel Double-core processor, CPU clocked frequency

at 2.7GHz, memory 4GB, and Window 10 operating system are sued. The computational complexity of the proposed method is slightly larger than the GFM, but its accuracy is much higher, demonstrated in Fig 9(a). Judging from both the performances improvement and computational complexity, the proposed method achieves a well trade-off.

B. REAL DATA RESULTS AND ANALYSIS

In this section, the airborne real data are utilized to demonstrate the effectiveness of the proposed method. The SAR data were collected by an airborne X-band radar system working at a broadside mode with parameters in Table 3.

Fig 10(a) depicts the SAR imaging result of the scene using the SPECAN algorithm [44], and it is seen that the moving targets are corrupted by strong clutter. The result of suppressing the clutter is shown in Fig 10(b), where the moving targets can be clearly seen, but they are smeared due to the RCM and DFM, demonstrated in Fig 10(c) that is enlarged part of the ellipse area in Fig 10(b). Due to the radial velocity, the moving targets are also displaced from the road where they should be. To clearly show the performances of different methods, one moving target in the ellipse is selected in Fig 10(c). The energy of this target spreads several range cells, and using PPFFT to estimate the slope of the trajectory, the range walk correction is realized, and the energy of the target is transformed into one range cell, shown in Fig 10(g).

In Fig 10(d)-(f), the range walk correction results of using KT method, RTM, and GFM are also provided for a comparison purpose. From the comparisons, they all transform the energy of the target into a range cell, but the proposed method produced a better performance.

After the RCM correction, with the CICPF, the energy of the moving target is accumulated as a sharp peak. From the peak position, the motion parameters are obtained to accomplish azimuth time-varying DFM compensation. Fig 10(h) provides the comparisons of range focusing results of moving
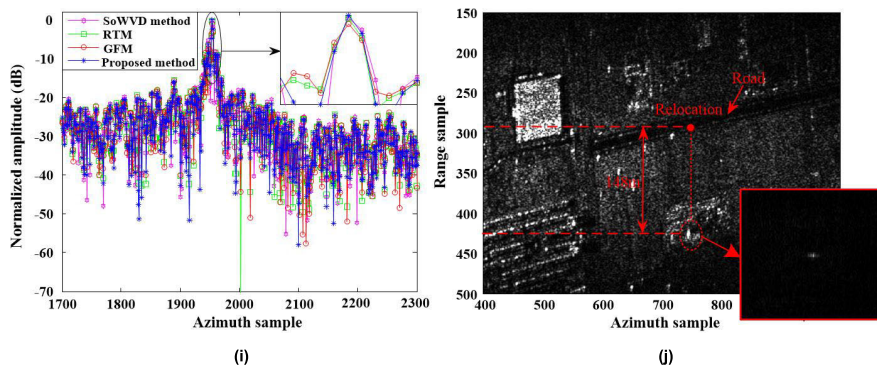

(a)

(b)

(c)

(d)

(e)

(f)

(g)

(h)
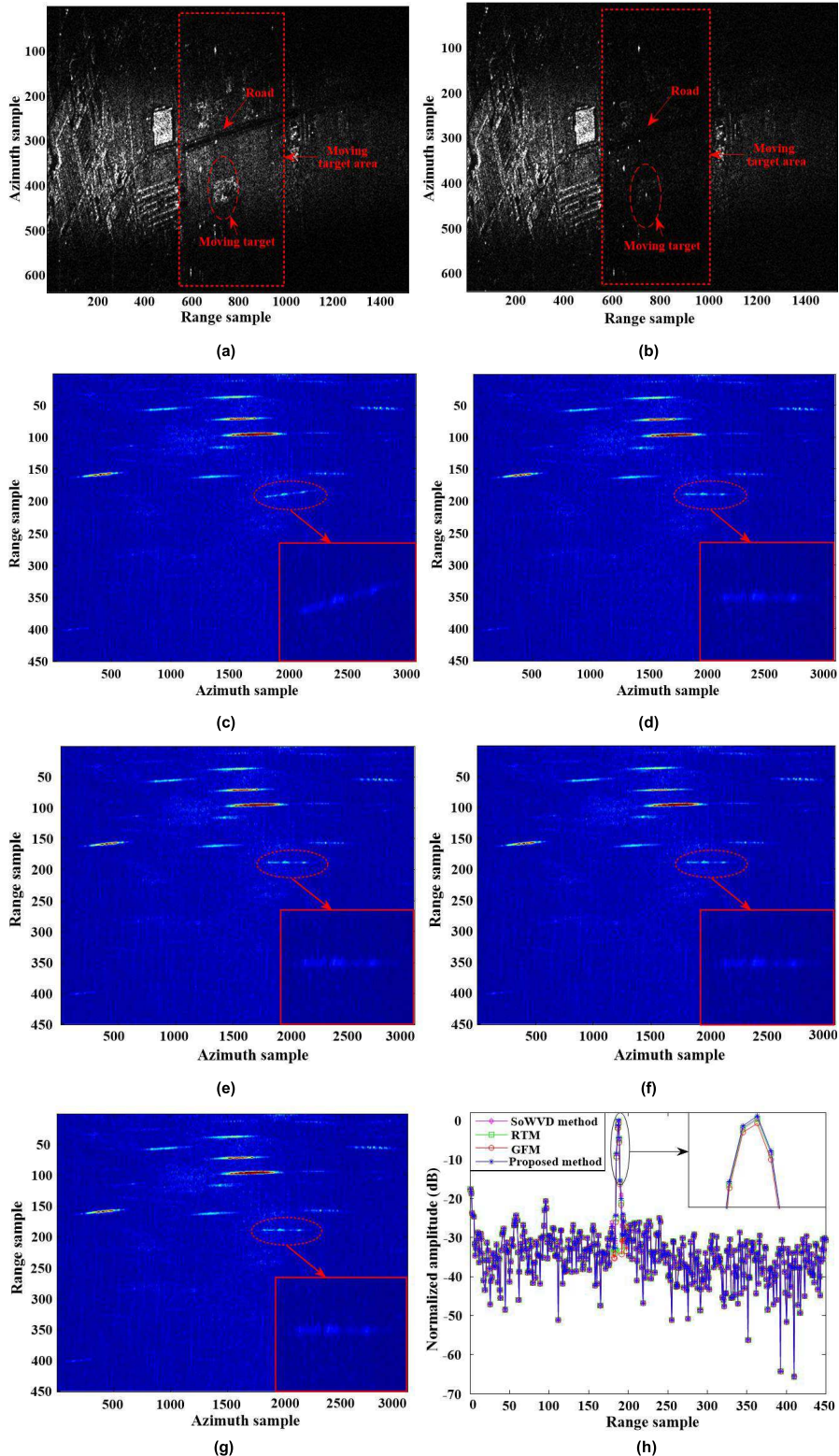
FIGURE 10. Imaging results of a ground moving target. (a) SAR image of the scene before clutter rejection. (b) SAR image of the scene after clutter suppression of moving target area. (c) The range walk of moving targets after clutter suppression. (d) The result of range walk correction using the KT method. (e) The result of range walk correction using the RT method. (f) The result of range walk correction using the GFM. (g)The result of range walk correction using the PPFFT method. (h) Comparison range focusing results of moving target by the SoWVD, RTM, GFM, and the proposed methods. (i) Comparison azimuth focusing results of moving target by the SoWVD method, RTM, GFM, and the proposed method. (j) Relocation results of the moving target.

target by SoWVD method, RTM, GFM, and the proposed method. Fig 10(i) shows the comparisons of azimuth focusing results of moving target by SoWVD method, RTM, GFM, and the proposed method. It is observed that the focus of the proposed method is slightly better than the existing methods. In Fig 10(j), with the estimated radial velocity of the proposed method, the moving target is accurately relocated on the original road. To summarize, from both the simulation and experimental experiments, the proposed method is highly desirable in SAR moving targets refocusing because its estimation accuracy high with a relatively low computational complexity.

V. CONCLUSION

This paper develops an efficient ground moving target refocusing method based on PPFFT and CICPF. First, using the known radar motion parameters, the range curvature correction is realized. Second, by a use of the efficient PPFFT, the slope of the range walk is estimated, and radial velocity of the moving target is thus obtained to complete the range walk correction. After that, the resulting signal is modeled as LFM signal and the CICPF is used to obtain the azimuth DFM parameters to produce well-focused result. The numerical studies including simulations and real data demonstrate the performance of the proposed method over the current existing approaches.

REFERENCES

[1] S. Zhu, G. Liao, H. Tao, Y. Qu, and Z. Yang, "Ground moving target detection and velocity estimation based on spatial multilook processing for multichannel airborne SAR," *IEEE Trans. Aerosp. Electron. Syst.*, vol. 49, no. 2, pp. 1322–1337, Apr. 2013.

[2] X. Zhang, G. Liao, S. Zhu, Y. Gao, and J. Xu, "Geometry-information-aided efficient motion parameter estimation for moving-target imaging and location," *IEEE Geosci. Remote Sens. Lett.*, vol. 12, no. 1, pp. 155–159, Jan. 2015.

[3] H. Liu, D. Li, Y. Zhou, and T.-K. Truong, "Simultaneous radio frequency and wideband interference suppression in SAR signals via sparsity exploitation in time–frequency domain," *IEEE Trans. Geosci. Remote Sens.*, vol. 56, no. 10, pp. 5780–5793, Oct. 2018.

[4] D. Henke, C. Magnard, M. Frioud, D. Small, E. Meier, and M. E. Schaepman, "Moving-target tracking in single-channel wide-beam SAR," *IEEE Trans. Geosci. Remote Sens.*, vol. 50, no. 11, pp. 4735–4747, Nov. 2012.

[5] M. Arii, "Efficient motion compensation of a moving object on SAR imagery based on velocity correlation function," *IEEE Trans. Geosci. Remote Sens.*, vol. 52, no. 2, pp. 936–946, Feb. 2014.

[6] E. C. Zaugg and D. G. Long, "Theory and application of motion compensation for LFM-CW SAR," *IEEE Trans. Geosci. Remote Sens.*, vol. 46, no. 10, pp. 2990–2998, Oct. 2008.

[7] R. P. Perry, R. C. Dipietro, and R. L. Fante, "SAR imaging of moving targets," *IEEE Trans. Aerosp. Electron. Syst.*, vol. 35, no. 1, pp. 188–200, Jan. 1999.

[8] D. Zhu, Y. Li, and Z. Zhu, "A keystone transform without interpolation for SAR ground moving-target imaging," *IEEE Geosci. Remote Sens. Lett.*, vol. 4, no. 1, pp. 18–22, Jan. 2007.

[9] P. Huang, G. Liao, Z. Yang, X.-G. Xia, J.-T. Ma, and X. Zhang, "A fast SAR imaging method for ground moving target using a second-order WVD transform," *IEEE Trans. Geosci. Remote Sens.*, vol. 54, no. 4, pp. 1940–1956, Apr. 2016.

[10] D. Kirkland, "Imaging moving targets using the second-order keystone transform," *IET Radar, Sonar Navigat.*, vol. 5, no. 8, pp. 902–910, Oct. 2011.

[11] J. Yang and Y. Zhang, "An airborne SAR moving target imaging and motion parameters estimation algorithm with azimuth-dechirping and the second-order keystone transform applied," *IEEE J. Sel. Topics Appl. Earth Observ. Remote Sens.*, vol. 8, no. 8, pp. 3967–3976, Aug. 2015.

[12] G. Li, X.-G. Xia, and Y.-N. Peng, "Doppler keystone transform: An approach suitable for parallel implementation of SAR moving target imaging," *IEEE Geosci. Remote Sens. Lett.*, vol. 5, no. 4, pp. 573–577, Oct. 2008.

[13] G. Sun, M. Xing, X.-G. Xia, Y. Wu, and Z. Bao, "Robust ground moving-target imaging using Deramp–Keystone processing," *IEEE Trans. Geosci. Remote Sens.*, vol. 51, no. 2, pp. 966–982, Feb. 2013.

[14] Y.-K. Kong, B.-L. Cho, and Y.-S. Kim, "Ambiguity-free Doppler centroid estimation technique for airborne SAR using the Radon transform," *IEEE Trans. Geosci. Remote Sens.*, vol. 43, no. 4, pp. 715–721, Apr. 2005.

[15] J. Xu, J. Yu, Y.-N. Peng, and X.-G. Xia, "Radon-Fourier transform for radar target detection, I: Generalized Doppler filter bank," *IEEE Trans. Aerosp. Electron. Syst.*, vol. 47, no. 2, pp. 1186–1202, Apr. 2011.

[16] X. Chen, J. Guan, N. Liu, and Y. He, "Maneuvering target detection via radon-fractional Fourier transform-based long-time coherent integration," *IEEE Trans. Signal Process.*, vol. 62, no. 4, pp. 939–953, Feb. 2014.

[17] M. R. Sharif and S. S. Abeysekera, "Efficient wideband signal parameter estimation using a radon-ambiguity transform slice," *IEEE Trans. Aerosp. Electron. Syst.*, vol. 43, no. 2, pp. 673–688, Apr. 2007.

[18] W.-C. Li, X.-S. Wang, and G.-Y. Wang, "Scaled radon-Wigner transform imaging and scaling of maneuvering target," *IEEE Trans. Aerosp. Electron. Syst.*, vol. 46, no. 4, pp. 2043–2051, Oct. 2010.

[19] P. R. Kersten, R. W. Jansen, K. Luc, and T. L. Ainsworth, "Motion analysis in SAR images of unfocused objects using time–frequency methods," *IEEE Geosci. Remote Sens. Lett.*, vol. 4, no. 4, pp. 527–531, Oct. 2007.

[20] X.-G. Xia and V. C. Chen, "A quantitative SNR analysis for the pseudo Wigner-Ville distribution," *IEEE Trans. Signal Process.*, vol. 47, no. 10, pp. 2891–2894, Oct. 1999.

[21] P. Huang, G. Liao, Z. Yang, X.-G. Xia, J. Ma, and J. Zheng, "Ground maneuvering target imaging and high-order motion parameter estimation based on second-order Keystone and generalized Hough-HAF transform," *IEEE Trans. Geosci. Remote Sens.*, vol. 55, no. 1, pp. 320–335, Jan. 2017.

[22] L. B. Almeida, "The fractional Fourier transform and time-frequency representations," *IEEE Trans. Signal Process.*, vol. 42, no. 11, pp. 3084–3091, Nov. 1994.

[23] H.-B. Sun, G.-S. Liu, H. Gu, and W.-M. Su, "Application of the fractional Fourier transform to moving target detection in airborne SAR," *IEEE Trans. Aerosp. Electron. Syst.*, vol. 38, no. 4, pp. 1416–1424, Oct. 2002.

[24] S. Zhu, G. Liao, Y. Qu, Z. Zhou, and X. Liu, "Ground moving targets imaging algorithm for synthetic aperture radar," *IEEE Trans. Geosci. Remote Sens.*, vol. 49, no. 1, pp. 462–477, Jan. 2011.

[25] X. Zhang, G. Liao, S. Zhu, C. Zeng, and Y. Shu, "Geometry-information-aided efficient radial velocity estimation for moving target imaging and location based on radon transform," *IEEE Trans. Geosci. Remote Sens.*, vol. 53, no. 2, pp. 1105–1117, Feb. 2015.

[26] G. Lv, Y. Li, G. Wang, and Y. Zhang, "Ground moving target indication in SAR images with symmetric Doppler views," *IEEE Trans. Geosci. Remote Sens.*, vol. 54, no. 1, pp. 533–543, Jan. 2016.

[27] Y. Zhao, S. Han, J. Yang, L. Zhang, H. Xu, and J. Wang, "A novel approach of slope detection combined with Lv's distribution for airborne SAR imagery of fast moving targets," *Remote Sens.*, vol. 10, no. 5, p. 764, May 2018.

[28] D. Li, M. Zhan, H. Liu, Y. Liao, and G. S. Liao, "A robust translational motion compensation method for ISAR imaging based on keystone transform and fractional Fourier transform under low SNR environment," *IEEE Trans. Aerosp. Electron. Syst.*, vol. 53, no. 5, pp. 2140–2156, Oct. 2017.

[29] J. Yang, C. Liu, and Y. Wang, "Detection and imaging of ground moving targets with real SAR data," *IEEE Trans. Geosci. Remote Sens.*, vol. 53, no. 2, pp. 920–932, Feb. 2015.

[30] B. Porat and B. Friedlander, "Asymptotic statistical analysis of the high-order ambiguity function for parameter estimation of polynomial-phase signals," *IEEE Trans. Inf. Theory*, vol. 42, no. 3, pp. 995–1001, May 1996.

[31] P. C. Suo, P. Tao, R. Tao, and Z. Nan, "Detection of high-speed and accelerated target based on the linear frequency modulation radar," *IET Radar Sonar Navigat.*, vol. 8, no. 1, pp. 37–47, Jan. 2014.

[32] X. Lv, G. Bi, C. Wan, and M. Xing, "Lv's distribution: Principle, implementation, properties, and performance," *IEEE Trans. Signal Process.*, vol. 59, no. 8, pp. 3576–3591, Aug. 2011.

[33] K. R. Varshney, M. Çetin, J. W. Fisher, and A. S. Willsky, "Sparse representation in structured dictionaries with application to synthetic aperture radar," *IEEE Trans. Signal Process.*, vol. 56, no. 8, pp. 3548–3561, Aug. 2008.

[34] Q. Wu, M. Xing, C. Qiu, B. Liu, Z. Bao, and T.-S. Yeo, "Motion parameter estimation in the SAR system with low PRF sampling," *IEEE Geosci. Remote Sens. Lett.*, vol. 7, no. 3, pp. 450–454, Jul. 2010.

[35] D. Li, X. Gui, H. Liu, J. Su, and H. Xiong, "An ISAR imaging algorithm for maneuvering targets with low SNR based on parameter estimation of multicomponent quadratic FM signals and nonuniform FFT," *IEEE J. Sel. Topics Appl. Earth Observ. Remote Sens.*, vol. 9, no. 12, pp. 5688–5702, Dec. 2016.

[36] P. Wang, I. Djurovic, and J. Yang, "Generalized high-order phase function for parameter estimation of polynomial phase signal," *IEEE Trans. Signal Process.*, vol. 56, no. 7, pp. 3023–3028, Jul. 2008.

[37] P. Wang and J. Y. Yang, "Multicomponent chirp signals analysis using product cubic phase function," *Digit. Signal Process.*, vol. 16, no. 6, pp. 654–669, Nov. 2006.

[38] P. Wang, H. Li, I. Djurovic, and B. Himed, "Integrated cubic phase function for linear FM signal analysis," *IEEE Trans. Aerosp. Electron. Syst.*, vol. 46, no. 3, pp. 963–977, Jul. 2010.

[39] S.-H. Park, H.-T. Kim, and K.-T. Kim, "Cross-range scaling algorithm for ISAR images using 2-D Fourier transform and polar mapping," *IEEE Trans. Geosci. Remote Sens.*, vol. 49, no. 2, pp. 868–877, Feb. 2011.

[40] A. Averbuch, R. R. Coifman, D. L. Donoho, M. Israeli, and J. Waldén, "Fast slant stack: A notion of radon transform for data in a Cartesian grid which is rapidly computible, algebraically exact, geometrically faithful and invertible," *J. Sci. Comput.*, vol. 37, no. 3, pp. 192–206, Jan. 2001.

[41] Y. Keller, Y. Shkolnisky, and A. Averbuch, "The angular difference function and its application to image registration," *IEEE Trans. Pattern Anal. Mach. Intell.*, vol. 27, no. 6, pp. 969–976, Jun. 2005.

[42] E. Sejdić, I. Djurović, and L. Stanković, "Fractional Fourier transform as a signal processing tool: An overview of recent developments," *Signal Process.*, vol. 91, no. 6, pp. 1351–1369, Jun. 2011.

[43] D. Li, M. Zhan, J. Su, H. Liu, and G. Liao, "Performances analysis of coherently integrated CPF for LFM signal under low SNR and its application to ground moving target imaging," *IEEE Trans. Geosci. Remote Sens.*, vol. 55, no. 11, pp. 6402–6419, Nov. 2017.

[44] I. G. Cumming and F. H. Wong, *Digital Processing of Synthetic Aperture Radar Data: Algorithms and Implementation*. Norwood, MA, USA: Artech House, 2005.

DONG LI (M'16–SM'19) was born in Inner Mongolia, China, in 1983. He received the B.S. degree in automation from the Chengdu University of Information Technology, Chengdu, China, in 2007, the M.S. degree in signal processing from Sichuan University, Chengdu, in 2010, and the Ph.D. degree in signal and information processing from the National Laboratory of Radar Signal Processing, Xidian University, Xi'an, China, in 2014.

He is currently an Associate Professor with the Center of Communication and Tracking Telemetering Command, Chongqing University, Chongqing, China. His research interests include SAR/ISAR imaging, moving target detection and recognition, and parameter estimation.

CHENGXIANG ZHANG was born in Henan, China, in 1990. He received the B.S. degree in electronic information science and technology from Nanjing Agricultural University, Nanjing, China, in 2017. He is currently pursuing the M.S. degree with the School of Microelectronics and Communication Engineering, Chongqing University, Chongqing, China.

His research interests include SAR/ISAR imaging and parameter estimation.

HAINING MA was born in Henan, China, in 1995. She received the B.S. degree in communication engineering from Henan University, Henan, China, in 2018. She is currently pursuing the M.S. degree with the School of Microelectronics and Communication Engineering, Chongqing University, Chongqing, China.

Her research interests include SAR moving target imaging and parameter estimation.

JIA SU (M'17) received the B.S. degree in communication engineering and the M.S. degree in optical communication from the Guilin University of Electronic Technology, Guilin, China, in 2008 and 2011, respectively, and the Ph.D. degree in signal and information processing from Xidian University, Xi'an, China, in 2015.

He is currently an Assistant Professor with the School of Electronics and Information, Northwestern Polytechnic University, Xi'an. His research interests include radar signal processing and time–frequency analysis.
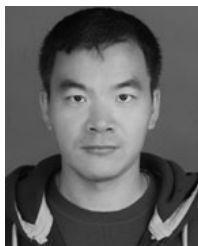
HONGQING LIU (M'15–SM'17) received the bachelor's and master's degrees from Xidian University, Xi'an, Shaanxi, China, in 2003 and 2006, respectively, and the Ph.D. degree from the City University of Hong Kong, Hong Kong, in 2009, all in electronic engineering.

He joined the Chongqing Key Laboratory of Mobile Communications Technology, Chongqing University of Posts and Telecommunications, Chongqing, China, in 2013, as a Faculty Member. His research interests include statistical signal processing and convex optimization, such as sparse signal reconstruction, localization/tracking, and parameter estimation.

QINGHUA LIU was born in Sichuan, China, in 1974. She received the B.S. degree in physics from Sichuan Normal University, Chengdu, China, in 1995, the M.S. degree in signal and information processing from the Guilin University of Electronic Technology, Guilin, China, in 2001, and the Ph.D. degree in signal and information processing from Xidian University, Xi'an, China, in 2014.

She is currently an Associate Professor with the School of Information and Communication, Guilin University of Electronic Technology. Her research interests include target detection and active noise control.

● ● ●